BioMedical Engineering OnLine

RESEARCH

Open Access

Experimental and computational evaluation of knee implant wear and creep under in vivo and ISO boundary conditions

Michael J. Dreyer[1,2], Seyyed Hamed Hosseini Nasab[1], Philippe Favre[3], Fabian Amstad[3], Rowena Crockett[4], William R. Taylor[1*] and Bernhard Weisse[2]

*Correspondence:
bt@ethz.ch

[1] Laboratory for Movement Biomechanics, Institute for Biomechanics, ETH Zürich, Gloriastrasse 37/39, 8092 Zurich, Switzerland
[2] Laboratory for Mechanical Systems Engineering, Empa, Dübendorf, Switzerland
[3] Zimmer Biomet, Zug, Switzerland
[4] Laboratory for Surface Science and Coating Technologies, Empa, Dübendorf, Switzerland

Abstract

Background: Experimental knee implant wear testing according to ISO 14243 is a standard procedure, but it inherently possesses limitations for preclinical evaluations due to extended testing periods and costly infrastructure. In an effort to overcome these limitations, we hereby develop and experimentally validate a finite-element (FE)-based algorithm, including a novel cross-shear and contact pressure dependent wear and creep model, and apply it towards understanding the sensitivity of wear outcomes to the applied boundary conditions.

Methods: Specifically, we investigated the application of in vivo data for level walking from the publicly available "Stan" data set, which contains single representative tibiofemoral loads and kinematics derived from in vivo measurements of six subjects, and compared wear outcomes against those obtained using the ISO standard boundary conditions. To provide validation of the numerical models, this comparison was reproduced experimentally on a six-station knee wear simulator over 5 million cycles, testing the same implant Stan's data was obtained from.

Results: Experimental implementation of Stan's boundary conditions in displacement control resulted in approximately three times higher wear rates (4.4 vs. 1.6 mm^3 per million cycles) and a more anterior wear pattern compared to the ISO standard in force control. While a force-controlled ISO FE model was unable to reproduce the bench test kinematics, and thus wear rate, due to a necessarily simplified representation of the simulator machine, similar but displacement-controlled FE models accurately predicted the laboratory wear tests for both ISO and Stan boundary conditions. The credibility of the in silico wear and creep model was further established per the ASME V&V-40 standard.

Conclusions: The FE wear model is suitable for supporting future patient-specific models and development of novel implant designs. Incorporating the Stan data set alongside ISO boundary conditions emphasized the value of using measured kinematics in displacement control for reliably replicating in vivo joint mechanics in wear simulation. Future work should focus on expanding the range of daily activities simulated and addressing model sensitivity to contact mechanics to further enhance predictive accuracy.

Keywords: Implant, Knee, Wear, Creep, Model, Simulation

Background

Longevity of knee implants is a major concern for the two-thirds of total knee arthroplasty (TKA) patients who are less than 65 years [1]. Today, long term failure of knee implants due to wear of the polyethylene (PE) inlay [2] or related to aseptic loosening [3, 4] still occurs, despite improvements in implant designs and material such as PE crosslinking.

Efforts to comprehensively investigate and subsequently increase the long-term wear resistance of knee implants, however, are somewhat constrained by the cost- and time-intensiveness of laboratory wear tests: a test running for five million cycles at 1 Hz takes approximately 4 months to complete [5]. Thus, experimental implant wear testing is not a practicable tool to compare more than a few conditions or designs at a time. Moreover, variability in the outcome wear measures can be considerable and repeatability may be challenging to achieve [6].

To provide a viable alternative, computational wear simulations, mostly based on deformable finite-element (FE) models, have been developed [7–9]. Such computational models have proven to strongly complement experimental testing by being orders of magnitude faster and not requiring dedicated personnel and infrastructure [10]. This allows evaluating the influence of parameters such as implant design, implant positioning, or loading conditions on wear, each taken individually or simultaneously in probabilistic studies [11]. However, for such models to be useful, their credibility must first be established [12].

When mechanical and in silico wear simulations aim to predict in vivo wear, applied loads and kinematics should be representative of in vivo conditions. While such data has historically been scarce, in vivo implant loads and kinematics have now been made publicly available as part of the CAMS-Knee data set [13]. More recently, the data from the 6 CAMS-Knee subjects were standardized into the single averaged "Stan" data set, and thus made accessible for mechanical wear simulation [14]. Interestingly, the commonly used ISO 14243-1 standard loads and kinematics [15], which were calculated from simplified models, were shown to differ from the Stan loads and kinematics measured in vivo for level walking.

In this exploratory study, we first aimed to develop and validate an advanced computational wear and creep model for predictions of how patient- and implant-specific factors impact PE inlay wear. To this end, a cross-shear and contact-pressure dependent wear model was combined with a novel creep prediction method. The necessary input material data was obtained from fully independent experimental studies. Second, the first comparison of wear resulting from the application of Stan's loads and kinematics to wear induced from the ISO standard boundary conditions (BCs) was performed using both computational simulation and experimental testing of wear.

Results

Three different sets of results were obtained: first the knee simulator test, second the corresponding FE models with the same input data, and third the FE models with kinematics input that was directly measured in the knee simulator test (Table 1). For each of the three sets, Stan's in vivo condition and for the standard ISO condition are reported.

Joint loads and kinematics

Stan BC vs. ISO BC

Comparing the outputs, the test and models with Stan's BCs exhibited higher peak axial forces (~ 3187 N vs. ~ 2600 N) and peak external moments (9.6–20.5 Nm vs. 1.9–7.1 Nm) than with the ISO BCs (Fig. 1). For the kinematics, however, Stan's BCs resulted in lower peak flexion angles (~ 49° vs. ~ 58°), tibial internal rotation angles (~ 3.9° vs. 7.5°–10.3°), and tibial anterior translation (0.6–0.7 mm vs. 4.1–5.5 mm) than the ISO BCs.

ISO BC: experiment vs. model

For the $ISO_{FC,exp,nom}$ test and $ISO_{FC,mod,nom}$ model with the same inputs, there was no more than 23 N difference in peak output AP force and 1 Nm in IE moment (Fig. 1). The kinematics peaks, however, deviated by up to 1.4 mm in the AP and up to 2.9° in the IE directions, especially during swing phase. Moreover, in the $ISO_{FC,exp,nom}$ test, the peak internal rotation and anterior translation values varied by up to 2.5° and 1 mm over the course of the test. When the test's experimentally measured kinematics were applied to the $ISO_{DC,mod,meas}$ model, tibial loads differed from the FC ISO standard input loads. Specifically, AP contact forces acted only posteriorly and exceeded 500 N, compared to 230 N in the anterior and 130 N in the posterior directions for the $ISO_{FC,exp,nom}$ test and $ISO_{FC,mod,nom}$ model with nominal ISO inputs. External moments of the $ISO_{DC,mod,meas}$ model were low, however, at only 1.9 Nm compared to 7.1 Nm in the wear test.

Stan BC: experiment vs. model

For the Stan DC test and two FE models, the output kinematics were in close agreement with differences in peak AP translation and internal rotation of less than 0.2 mm and 0.1°. In contrast, load deviations between the experiment and the DC models were observed. Mostly anterior tibial forces of up to 93.5 N were observed experimentally, while both the $Stan_{DC,mod,nom}$ and $Stan_{DC,mod,meas}$ models predicted mostly

Table 1 Overview of experimental and modelling boundary conditions

Name ($BC_{mode,type,input}$)	Condition	Control mode	Description of type and input	Range of input tibial load/kinematics values
$ISO_{FC,exp,nom}$	ISO 14234-1 (2009)	Force (FC)	Bench test with nominal inputs	Flexion angle: 0 to 58° Axial force: 168 to 2600 N Anterior force: − 110 to 265 N Internal moment: − 6 to 1 Nm
$ISO_{FC,mod,nom}$			FE model with nominal inputs	
$ISO_{DC,mod,meas}$		Displacement (DC)	FE model with bench test measured loads/kinematics	See $ISO_{FC,exp,nom}$ in Fig. 1
$Stan_{DC,exp,nom}$	Stan level walking		Bench test with nominal inputs	Flexion angle: − 2° to 48° Axial force: 245 to 3187 N Anterior motion: − 5.1 to 0.7 mm Internal rotation: − 0.1° to 4.0°
$Stan_{DC,mod,nom}$			FE model with nominal inputs	
$Stan_{DC,mod,meas}$			FE model with bench test measured loads/kinematics	See $Stan_{DC,exp,nom}$ in Fig. 1

Note that flexion angle and axial force are driven in displacement and force control, respectively, for all tests regardless of the stated control mode, for consistency with ISO standards

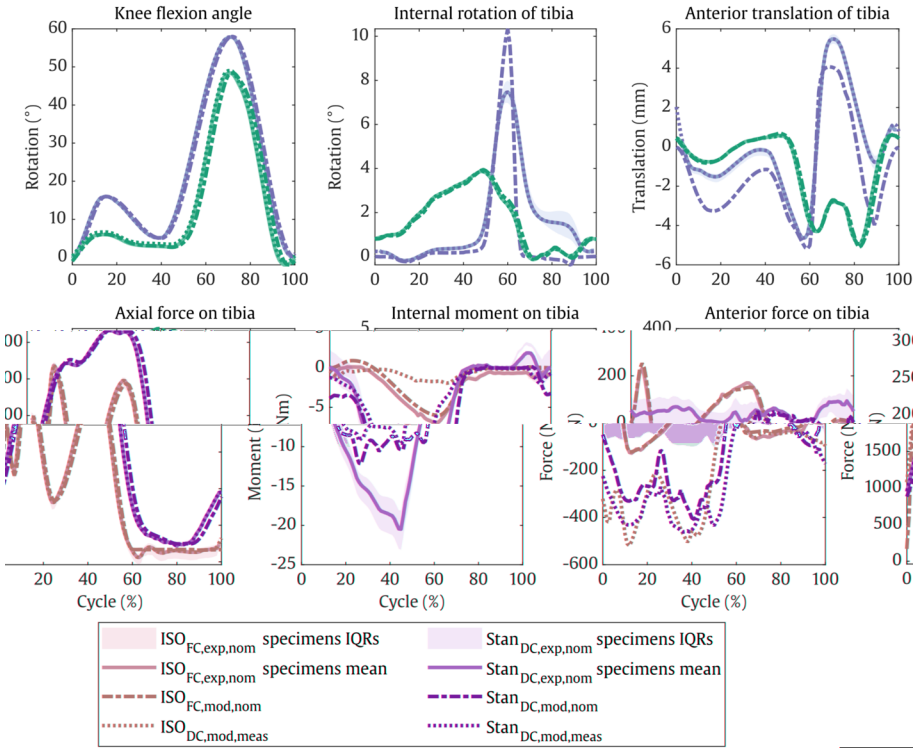

Fig. 1 Resulting joint loads and kinematics measured for the specimens on the simulator (mean over all test intervals and specimens and interquartile ranges (IQRs) of each specimen), simulated using finite-element analysis with the same inputs ($ISO_{FC,exp,nom}$ and $Stan_{DC,exp,nom}$), and simulated using the experimentally measured kinematics as input to the FE model ($ISO_{DC,exp,meas}$ and $Stan_{DC,exp}$). Forces and moments are expressed as external loads acting on the articulating surface of the tibial inlay

posterior forces of up to 408 N and 461 N, respectively (Fig. 1). Again, the modelled external moments of up to 12.2 Nm were lower compared to up to 20.4 Nm measured in the wear test. Moreover, in the $Stan_{DC,exp,nom}$ test, the peak internal moments and anterior forces varied by up to 8 Nm and 200 N over the course of the test.

Wear

During pre-soaking, the test samples gained 5.4–6.6 mg of weight in 12 weeks, while during the subsequent test, the loaded soak controls gained between 6.0 and 8.5 mg of weight in only 10 weeks. The experimentally measured linear volumetric wear rate from 0.5 to 5.0 MC was 1.3–1.9 mm^3/MC for the $ISO_{FC,exp,nom}$ group and a more than two-and-a-half times higher 3.5–4.9 mm^3/MC for the $Stan_{DC,exp,nom}$ group (Fig. 2). The $Stan_{DC,mod,nom}$ model predicted a wear rate of 4.3 mm^3/MC, falling well within the experimental range for these BCs. This was not the case for the $ISO_{FC,mod,nom}$ model, which predicted a wear rate of 4.8 mm^3/MC, being about three times higher than the corresponding experimentally obtained values. In contrast, both the $ISO_{DC,mod,meas}$ and $Stan_{DC,mod,meas}$ models driven by the experimental kinematics predicted wear rates that fell within the experimental ranges at 1.6 and 3.5 mm^3/MC, respectively (Fig. 2).

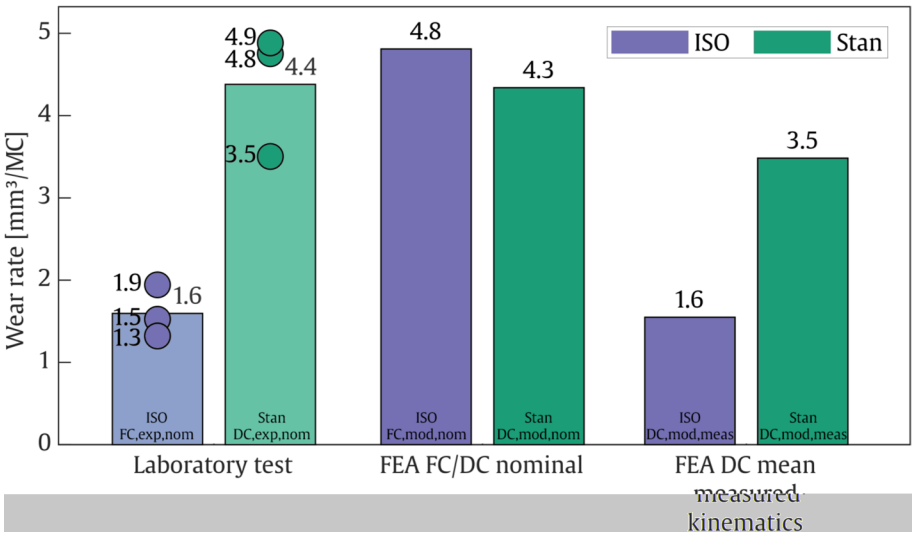

Fig. 2 Wear rates measured for the specimens on the simulator (Laboratory test), simulated using finite-element analysis with the same inputs (FEA FC/DC nominal), and simulated using the experimentally measured kinematics as inputs to the FE model (FEA DC mean measured kinematics)

Surface deformation

The $ISO_{FC,exp,nom}$ test induced clear surface deformation to the medial and posterior facets of the inlay, even though the overall wear rate was lower than for $Stan_{DC,exp,nom}$ (Fig. 3). The $ISO_{DC,mod,meas}$ model with the same kinematics showed similarly posterior, but less pronounced, surface deformation, while the $ISO_{FC,mod,nom}$ model showed posterolateral and anteromedial surface deformation. For the DC Stan condition, there was negative posterolateral and central medial surface deformation and slight positive lateral deformation in the laboratory test and both models. Concentrated anterior edge deformations were observed in both tests, while the corresponding models showed smaller and more distributed downwards deformations. Overall, the combined surface deformation induced by wear and creep in the FE simulations did not show the same pronounced edge deformations, but otherwise showed qualitatively similar trends compared to the 3D scan measurements on the corresponding physical test specimens.

Verification and validation

The credibility of the verification and validation activities was evaluated in accordance with standardized (ASME V&V 40) [16] and regulatory (FDA) [17] guidance on model credibility (see "Additional file 1"). The conclusion from this assessment (Fig. 4) was that the modeling approach here is credible for use in support of low-to-medium model risk applications when tests and models are run in DC mode.

Discussion

Laboratory-based testing of knee implant wear based on the currently established ISO boundary conditions is expensive and time consuming. Therefore, laboratory wear testing is rarely feasible for larger scale investigations into the effect of implant

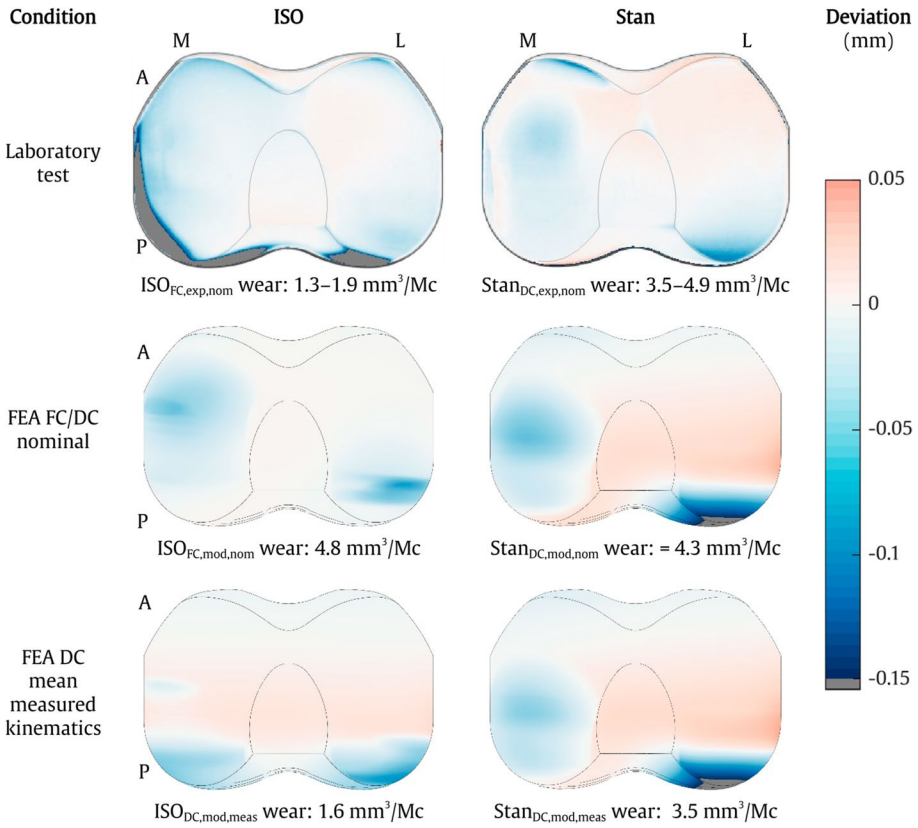

Fig. 3 Surface deviation in the axial direction caused by wear and creep after 5 MC for the four models and the test specimens. Each test specimen plot represents the mean deviation of the three corresponding specimens

design, patient or surgical factors, or activity on implant wear. In an effort to address this challenge, the efficacy of FE simulation coupled with advanced PE wear and creep models as an alternative method of wear quantification was demonstrated here. Systematic model verification and validation was carried out, and the first comparison of the recently published standardized tibiofemoral implant loads and kinematics ["Stan", 14] against the ISO boundary condition was performed. To our knowledge, this is also the first study investigating wear of the Innex knee implant by means of laboratory testing or computational modelling, hence providing quantitative evidence supporting the widely used CAMS-Knee data sets [13].

The main finding was that Stan's loads and kinematics resulted in higher wear rates and different surface deformation patterns compared to the ISO FC standard. Moreover, the FE wear model was able to accurately predict experimentally obtained wear, but was shown to be sensitive to inaccurate calculation of the joint kinematics. The experimental wear rates of 1.3–1.9 mm^3/MC for the ISO$_{FC,exp,nom}$ test and 3.5–4.9 mm^3/MC for the Stan$_{DC,exp,nom}$ test were lower than expected, however, compared to 5–40 mm^3/MC for various other knee implant models with inlays made from conventional non highly crosslinked PE [18]. The wear occurring more anteriorly on the medial than on the lateral condyle is consistent with earlier investigations of

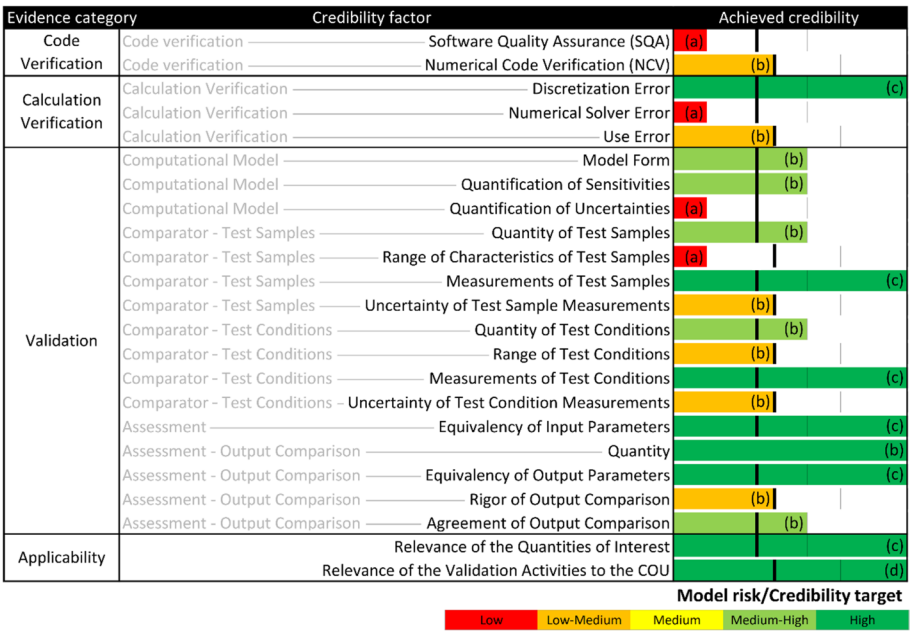

Fig. 4 Achieved FE wear model credibility for all credibility factors, inspired by the example proposed in the recent FDA draft guidance document [17]. The color coding and length of the horizontal bars indicate the achieved level of credibility, and the vertical black line segments indicate the model risk/credibility target. Mapping the variable 2 to 4 level gradation from the ASME V&V 40 [16] to a five-level gradation scheme from the FDA required an adaptation of the model risk/credibility target line to each credibility factor

tibiofemoral contact locations for the CAMS-Knee data on the same implant model [19] and of wear for similar in vivo data on another implant design [20].

The low wear rate of the $ISO_{FC,exp,nom}$ experiment can be explained by the contact occurring mainly on the posterior inlay edge. This is evident from the visible deformation for both the $ISO_{DC,mod,meas}$ model and the 3D scans (Fig. 3). The posterior contact led to a small contact area, resulting in little overall implant wear. In comparison, the $ISO_{FC,mod,nom}$ model with nominal inputs predicted contact to occur roughly 2 mm more anteriorly on the inlay (Fig. 1, top right). This resulted in a larger contact area (Fig. 3, middle left), more relative sliding and less rolling, and almost three times more wear (Fig. 2), as a larger contact area can increase wear even with the same load applied [7, 21, 22]. The large wear rate mismatch between the $ISO_{FC,mod,nom}$ model and the corresponding $ISO_{FC,exp,nom}$ experiment could therefore be due to limited representation of the simulator machine's inertial, friction, and control properties in the FC FE model, limiting its predictive capabilities with respect to joint kinematics. This is a common limitation of FC computational models [23–25] and does not necessarily indicate poor modelling of the wear mechanism itself.

Wear predicted by our algorithm in the DC models driven by nominal ($Stan_{DC,mod,nom}$) and measured ($ISO_{DC,mod,meas}$ and $Stan_{DC,mod,meas}$) kinematics accurately predicted wear rates within the range of experimentally measured values. The experimental surface wear patterns were more spread out than the model predictions and showed concentrated edge deformations. This is likely due to the observed variability in kinematics over the course of the test and for the $ISO_{DC,exp,nom}$ specimens due to an unwanted motion that occurred once after a test restart and deformed the inlay edges. However,

the surface deformation patterns still qualitatively matched the three DC models. All this was achieved without tuning the models' underlying material data to the validation experiments in any way, rather the material data was obtained from separate experiments. Wear volume and pattern were inaccurately predicted only for the $ISO_{FC,mod,nom}$ model, where the joint kinematics differed most compared to the experiment. This shows that knee implant wear can be predicted accurately if the underlying joint model is able to reliably reproduce the real-world joint contact mechanics, but may be inaccurate if not, highlighting the importance of exact in vivo measurements of joint kinematics for patient-specific models.

Specifically, accurate kinematics seem to be of higher importance for wear prediction than accurate loads. As discussed above, the $ISO_{FC,mod,nom}$ models' output kinematics deviated from the ones measured in the experiment by only a few mm/degrees but resulted in a threefold difference in wear rate. In contrast, the $Stan_{DC,mod,nom}$ model's loads deviated from the experiment by a factor of two for the internal moment and four for the anterior force, but still predicted wear rates accurately. The relatively large axial force is likely the main load driver for wear, while transverse load errors in DC models are less consequential. Reinforcing this deduction, other studies have also shown that variations in the joint kinematics, e.g., in AP and IE directions [26] had a larger impact on wear predictions than changes in the applied AP and IE loads [11, 27]. Hence, future application of WearPy is recommended with DC models, which the V&V activities were also focused on and showed credibility of.

Applying the Stan kinematics and associated CAMS-HIGH100 loads resulted in almost three times more wear than applying the ISO FC boundary conditions. While this is the first wear simulation study using the recently published Stan data set, others have applied in vivo loads collected earlier from some of the same subjects with instrumented implants in FC mode. The reported wear rates, compared to the ISO FC BCs, exhibited large variability, going from comparable [20], slightly higher [28], to up to three times higher [29]. However, such comparisons between test standards may not necessarily yield the same results for other implant designs [23], prohibiting a general interpretation of these results. Yet, while the body of evidence is still small, these and this study's results suggest that wear testing boundary conditions derived from in vivo measurements induce more wear than the standard ISO FC conditions.

A limitation of this study is that only one ultra-congruent implant design in one combination of component sizes and two sets of boundary conditions with different control methods were investigated. Further investigation of other implant designs and boundary conditions, e.g., the DC ISO standard and Stan's other activities of daily living, should be considered to more comprehensively investigate the effects of BCs derived from in vivo measurements on wear testing outcomes. Furthermore, the FE models presented here did not model the variability in component positioning, loads, kinematics, and geometry, which is unavoidable on a knee simulator, and thus did not account for rare extreme motions and their possible impact on surface and edge deformations and wear rates. Only the articulating surface was considered and only abrasive wear was modelled. The size of the contact patches was not measured experimentally, so no validation of the modelled contact area, which may have influenced predicted wear rates, was possible. Lastly, the PE material density and creep model were not obtained for the specific PE

material investigated here. Notwithstanding these limitations, the experimental wear rates were accurately reproduced by the FE models, which were based on independent prior studies of PE mechanical properties and wear.

We recommend that future computational wear simulation studies not only use in vivo kinematics, but also consider multiple activities of daily living [28, 29] and incorporate uncertainty in their evaluation to account for the sensitivity of wear models to variations in contact mechanics. This could be achieved using available standardized BCs [14, 30–32] complemented with a sensitivity analysis [11] or by modelling wear using data of multiple patients and trials [13, 33]. To make these rich data sets accessible for preclinical evaluation of implant wear, e.g., for different implant designs and patient-specific factors, the validated WearPy software is available upon request at https://www.empa.ch/web/s304/wearpy.

Conclusion

This study utilized finite-element simulation combined with advanced polyethylene wear and creep models as a viable alternative to traditional laboratory testing for quantifying knee implant wear. The first application of the novel "Stan" data set alongside the established ISO boundary conditions revealed higher wear rates for Stan's in vivo boundary conditions. Model verification and validation was performed in accordance with ASME V&V 40 and revealed that accurate joint kinematics are crucial for reliable computational wear prediction. Moving forward, incorporating a broader spectrum of activities of daily living and addressing model sensitivity to variations in contact mechanics through comprehensive simulations and uncertainty analysis will be essential to further enhance the predictive accuracy of wear models.

Methods

Wear test

Related to the first aim of the study, the main purpose of the experimental wear test was to validate the computational wear and creep model (see below). In addition, it served to compare the effect of the two different BCs on wear for the second aim of this study. For consistency, all experiments and computational simulations were performed on the same ultra-congruent cruciate-sacrificing TKA implant (Innex® FIXUC, Zimmer Biomet, Switzerland), which was also implanted in the patients involved in the CAMS-Knee and Stan investigations.

Implant components were tested on a six-station knee simulator (AMTI, Watertown, USA), which allowed control of femoral flexion angle and anterior–posterior (AP) force or translation, as well as tibial axial force and internal–external (IE) moment or rotation (Fig. 5). The tibial component was fixed to have a posterior slope of 6° according to the manufacturer's surgical technique.

The test lubricant was bovine calf serum (Hyclone™ Calf Serum, Cytvia, USA) diluted to a protein concentration of 20 g/L [ISO 14243-1, 15]. In addition, 7.4 g/L ethylenediaminetetraacetic acid disodium salt dihydrate (Fisher Scientific, USA) and 2.0 g/L sodium azide (Fisher Scientific, USA) were added to hinder bacterial growth and build-up of calcium phosphate on the implant surfaces according to ASTM

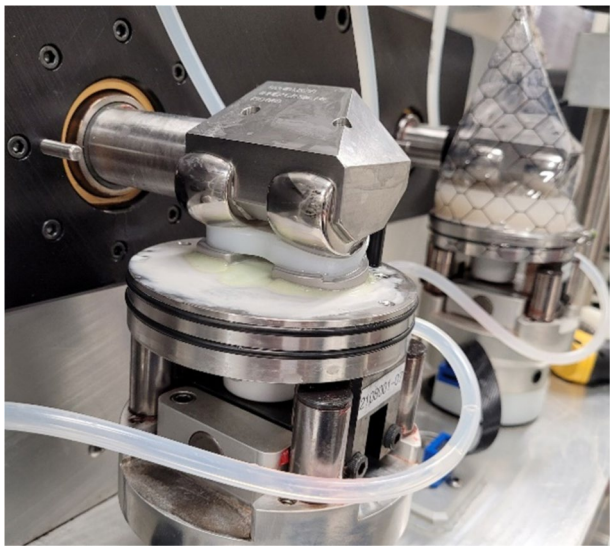

Fig. 5 Wear test specimens consisting of PE inlay, tibial, and femoral components fixed in the bench test setup in dry (foreground) and sealed with lubricant (background) state

F732-17 [34]. The specimens were pre-soaked in this lubricant for 12 weeks prior to testing which surpassed recommended minimum durations [35].

In the bench test setup (Fig. 5), the ISO BCs as well as Stan's kinematics for level walking and the associated CAMS-HIGH100 loads [14] were applied to the implants (Table 1). Stan's data were applied in displacement-control (DC) to closely reproduce the in vivo contact mechanics in the bench test and models. For consistency, Stan's conditions would ideally have been compared to the DC ISO 14243-3:2014 standard. However, preliminary FE simulation of the DC ISO standard showed excessive posterior edge loading, also observed in other studies [23, 36], which led to dislocation of the implant. Therefore, the force-controlled (FC) ISO 14243-1:2009 standard was used as a comparison for Stan's loads and kinematics.

One group of three specimens was subjected to the ISO FC BCs and one group of three specimens was subjected to Stan's kinematics in DC mode ($ISO_{FC,exp,nom}$ and $Stan_{DC,exp,nom}$ in Table 1, respectively). The ISO AP force, IE moment, and flexion angle were applied as per the FC standard [ISO 14243-1, 15]. Stan's CAMS-HIGH100 loads and kinematics were transformed to the ISO coordinate system and AP and IE kinematics (DC mode) and axial force were applied consistent with the DC ISO standard [ISO 14243-3, 37]. For each group, two additional soak-control specimens were submerged in lubricant and subjected to the same axial load profile as the wear specimens, but without any other loads or motion, to correct for PE weight changes due to fluid uptake.

The test was performed at 1.1 Hz for 5 million cycles (MC). Wear was measured gravimetrically at 500,000 cycles and afterwards at every full MC until test completion. Subsequently, the volumetric wear rate of each PE inlay was calculated from the slope of the regression line fitted to the wear volume over number of cycles, assuming a PE density of 0.935 g/cm^3 [38]. The effective loads and kinematics applied by the testing machine to the implants were recorded every 20,000 cycles to allow the average applied loads and kinematics to be calculated.

Before and after the test, the three-dimensional inlay geometry was measured using a structured light 3D scanner (Pro S3, HP Inc., USA) with a resolution of ~ 50 µm. Using custom Python scripts, the untested and tested 3D geometries of each specimen were aligned using an iterative closest point algorithm by first aligning the whole geometries and then only the flat intercondylar plateaus. Subsequently, the change in surface geometry due to wear and creep was calculated from the remaining deviations between the aligned scans.

Finite-element model

Finite-element (FE) models of the experimental test setup (Fig. 6) were created in Abaqus/Standard 6.21 (Dassault Systèmes, USA). These models consisted of the PE inlay and the femoral component, with tibio-femoral contact defined by a coefficient of friction of 0.04 [39]. The tibial component was not modelled, as the predicted backside wear on the fixed inlay would be minimal [40]. To enable roughly two times faster convergence, automatic tangential contact damping was activated, but scaled down by a factor of 0.0001 after confirming a negligible (< 0.4 mm) impact on model output kinematics. The inlay was assigned elastic–plastic material properties calibrated by the manufacturer to material characterization tests on the PE used in the Innex implant. Element size was chosen based on a convergence study on contact pressure and wear, reaching a change in output < 2% between two successive mesh refinements.

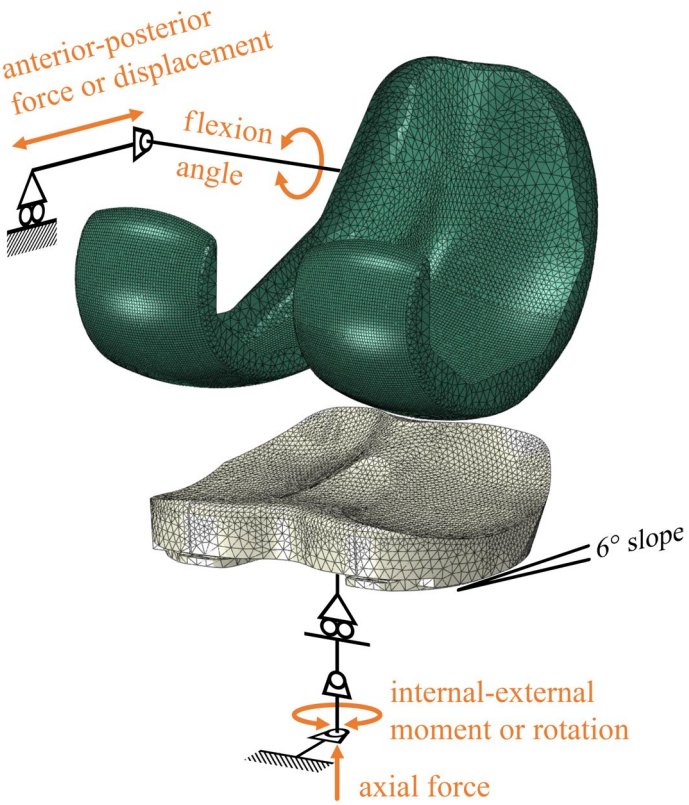

Fig. 6 Exploded view of the finite-element model, consisting of the inlay (beige) and femoral (green) components and the rigid connector elements representing the wear simulator fixtures

The inlay was assigned a general element size of 2.5 mm, with 0.9 mm elements on the contact surfaces, resulting in 41,833 quadratic tetrahedral elements. The femoral component was modelled as a rigid shell [41] with an element size of 0.5 mm on the contact surfaces and approximately 2 mm on the sides, for a total 22,764 linear quadrilateral and triangular elements. The testing machine's fixtures were represented by rigid connector elements (Fig. 6) to which the Stan and ISO input loads and kinematics were then applied, resulting in the $ISO_{FC,mod,nom}$ and $Stan_{DC,mod,nom}$ models (Table 1). Each boundary condition motion cycle was split into 200 time intervals, based on a temporal convergence study considering volumetric wear, leading to a difference of < 0.2% between two interval sizes.

For the same input loads or kinematics, slightly different resultant contact loads and kinematics could be expected between the knee simulator, which is affected by inertia, tolerances, and control system delays, and the FE model, which is affected by simplifications and idealized component geometries. This is especially the case for FC mode, where deviations of several millimetres and degrees commonly occur [23–25]. To evaluate the influence of these different contact mechanics on wear and creep prediction, two additional simulations were run. Specifically, the average kinematics and axial forces of the ISO and Stan groups measured on the testing machine were applied to the corresponding FE models in DC mode ($ISO_{DC,mod,meas}$ and $Stan_{DC,mod,meas}$ in Table 1). In this manner, the wear rates of the FE model and experiment were evaluated under identical contact kinematics.

Wear and creep prediction algorithm

Implant wear is known to depend on contact mechanics, but contact mechanics progressively change if the surface geometry is altered by wear or creep [42]. To ensure appropriate modelling of wear [25, 43], this interdependence was reproduced iteratively in our wear and creep prediction algorithm (named "WearPy"), a custom Python code that directly interacts with Abaqus (Fig. 7).

WearPy divides the total number of cycles n_{max} (5 MC here) into steps of fewer cycles n_{inc}. Each step consists of the solution of the FE model described above for a single motion cycle, the calculation of wear and surface loads from the results, and the extrapolation of the wear and simulation of the creep over n_{inc} cycles until the next step. The removal of material due to wear and the deformation due to creep are modeled by updating the surface nodal positions. A preliminary convergence study on a model of a half-sphere against a flat disk showed that a change in surface geometry of up to 0.01 mm would not significantly change the contact mechanics. Thus, to ensure a smooth progression of surface deformation [43], WearPy automatically chose the largest possible number of cycles per step (n_{inc}) such that the larger of wear and creep caused surface deformations of exactly 0.01 mm and the smaller of wear and creep consequently caused < 0.01 mm of deformation. After calculating a step wear and creep for the chosen number of cycles, the inlay mesh was updated, and the whole procedure was repeated until $n_{max} = 5$ MC was reached. Depending on the boundary conditions, 13–19 iterations using n_{inc} values of as low as 990 (first iteration with most creep) to 719,000 (last iteration, wear) cycles were simulated which took roughly 4 days on a workstation computer.

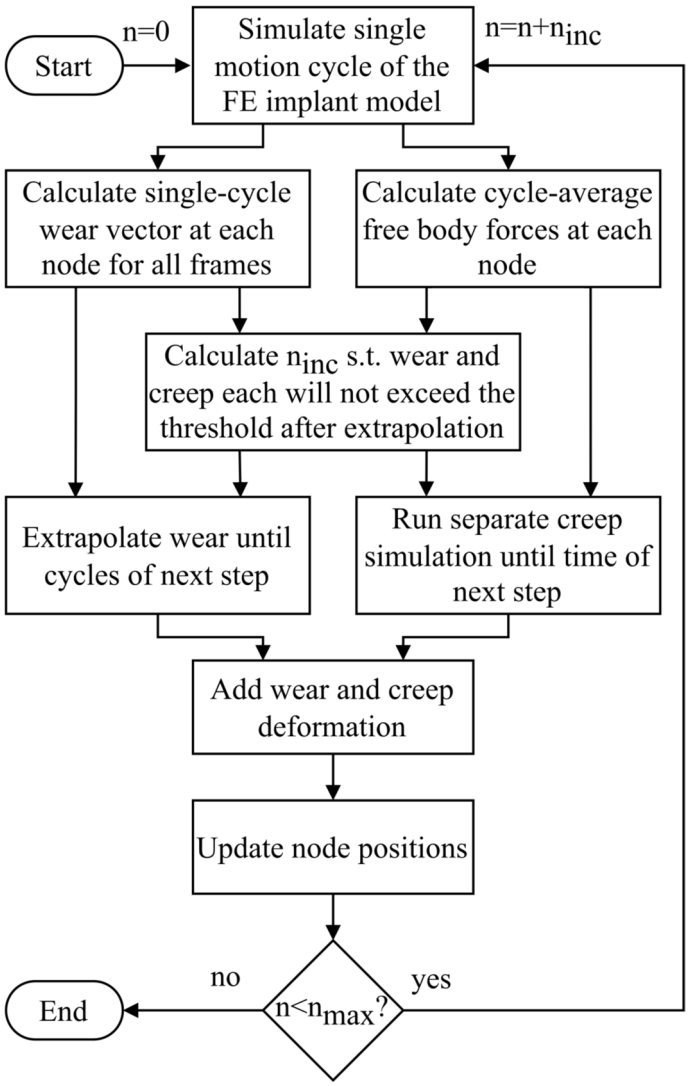

Fig. 7 Flowchart of the "WearPy" implant wear and creep prediction pipeline. Here, n represents the current number of cycles in the analysis, which is iterative with steps of fewer cycles n_{inc} and stops when the maximum number of cycles n_{max} is reached

Wear model

To model the critical influence of cross-shear and contact-pressure on wear [44], the local wear depth δ at each node was calculated using a modified version of Archard's law:

$$\delta = k(\mathrm{CS}, \mathrm{CP}) \times \mathrm{CP} \times \Delta x.$$

Here, Δx is the sliding distance, and k(CS,CP), measured in $\mathrm{mm}^3\,\mathrm{N}^{-1}\,\mathrm{m}^{-1}$, is the wear factor as a function of contact-pressure CP and a cross-shear ratio CS [45, (Eqs. 4–8)] based on the commonly adopted concept of frictional work [46]. The wear factor k(CS,CP) was defined as

$$k(\mathrm{CS}, \mathrm{CP}) = 10^{-6} \times (0.0202 + 0.888 \times (1 - \exp(-50.9 \times \mathrm{CS}))) \times \mathrm{CP}^{-0.649}.$$

This empirical expression was derived from comprehensive pin-on-disk wear tests performed on the same PE material from which the inlays in this study are made [47] and is similar to other published wear equations (Supplementary Figure S2 in "Additional file 1").

Creep model

To improve the accuracy of the contact-pressure dependent wear model, it is necessary to include surface deformations due to creep in the model [48]. Thus, a model for dynamic compressive creep of PE from the literature [49] was adapted, assuming 50% of creep deformation would be recovered [50] during the test interruptions to measure gravimetric wear as well as after the test. The formula to calculate the creep strain ε_{creep} based on the von-Mises stress σ_{VM} and the time in minutes, $t_{minutes}$, was defined as

$$\varepsilon_{creep} = \left(2.076 \times 10^{-3} + 3.897 \times 10^{-4} \times \left(\log_{10}(t_{minutes}) - 4\right)\right) \times \frac{\sigma_{VM}}{0.55} \times 0.5.$$

This equation was implemented into the Abaqus "CREEP" user-subroutine. As part of the wear prediction algorithm, a separate creep analysis was automatically performed to determine the geometrical changes that occur over the number of cycles n_{inc} between two steps. During this creep analysis, the average over time of all the free-body-forces from contact and boundary conditions acting on each node of the inlay during the motion cycle was extracted from the solution of the FE model described above and then, in a separate creep simulation, applied as a static load to each node of the inlay. Thus, creep deformation was calculated for the whole inlay. To our knowledge, this is the first study to consider creep of a whole knee implant component, as other studies only modelled creep in a local contact area [6, 8, 43, 51].

Verification and validation

To assess the credibility of the modelling approach and WearPy, verification and validation was performed according to ASME V&V 40-2018 [16] and FDA [17] guidelines (see "Additional file 1"). To this end, the verification included comparisons of the wear and creep predicted in simplified pin-on-disk models to the analytical solutions as well as various convergence analyses. The validation included a comparison of the FE models and the experimental test comparator for the ISO and Stan conditions. A hypothetical context of use was defined, where the wear would be predicted during development of a new knee implant to identify the worst-case configuration for experimental wear testing. Finally, each of the credibility factors was independently assessed relative to the model risk associated with using the model here to support comparative evaluation of TKA designs.

Supplementary Information

The online version contains supplementary material available at https://doi.org/10.1186/s12938-024-01321-0.

Additional file 1: Contains an assessment of the credibility of computational *WearPy* wear models per the ASME V&V 40 standard and a comparison of published empirical wear formulas.

Acknowledgements
We would like to thank Zimmer Biomet for providing access to the INNEX implant CAD files and PE material data, for providing material samples and implant components, and for running the physical test on the knee simulator. We would also like to thank Jeff Bischoff for his help with the verification and validation standards. We would like to thank Zimmer Biomet for providing access to the INNEX implant CAD files and PE material data, for providing material samples and implant components, and for running the physical test on the knee simulator. We would also like to thank Jeff Bischoff for his help with the verification and validation standards.

Author contributions
Conceptualization: MJD, SHHN, WRT, and BW. Data curation: MJD and FA. Formal analysis: MJD. Funding acquisition: PF, RC, WRT, and BW. Investigation: MJD and FA. Methodology: MJD and SHHN. Project administration: PF, FA, and BW. Resources: PF and FA. Software: MJD. Supervision: WRT and BW. Validation: MJD and PF. Visualization: MJD. Writing—original draft: MJD. Writing—review and editing: MJD, SHHN, PF, FA, RC, WRT, and BW.

Funding
Open access funding provided by Swiss Federal Institute of Technology Zurich. This research was supported by Empa, ETH Zurich, and Zimmer Biomet.

Availability of data and materials
The Stan data set supporting the conclusions of this article is available upon request for research purposes in the CAMS-Knee repository, https://cams-knee.orthoload.com/data/data-request/. The WearPy software is available upon request at https://www.empa.ch/web/s304/wearpy.

Declarations

Ethics approval and consent to participate
Not applicable.

Consent for publication
Not applicable.

Competing interests
MJD, SHHN, BW, and WRT declare that they have no known competing financial interests or personal relationships that could have appeared to influence the work reported in this paper. PF and FA are employed at Zimmer Biomet, the company producing the Innex implant investigated here.

Received: 26 August 2024 Accepted: 9 December 2024
Published online: 23 December 2024

References

1. Kurtz SM, Lau E, Ong K, Zhao K, Kelly M, Bozic KJ. Future young patient demand for primary and revision joint replacement: national projections from 2010 to 2030. Clin Orthop Relat Res. 2009;467:2606–12.
2. Kim KT, Lee S, Ko DO, Seo BS, Jung WS, Chang BK. Causes of failure after total knee arthroplasty in osteoarthritis patients 55 years of age or younger. Knee Surg Relat Res. 2014;26:13–9.
3. Pitta M, Esposito CI, Li Z, Lee Y, Wright TM, Padgett DE. Failure after modern total knee arthroplasty: a prospective study of 18,065 knees. J Arthroplasty. 2018;33:407–14.
4. Oparaugo PC, Clarke IC, Malchau H, Herberts P. Correlation of wear debris-induced osteolysis and revision with volumetric wear-rates of polyethylene: a survey of 8 reports in the literature. Acta Orthop Scand. 2001;72:22–8.
5. Haider H. Chapter-26 Tribological assessment of UHMWPE in the knee. In: Kurtz SM, editor. UHMWPE Biomater Handbook. 2nd ed. Boston: Academic Press; 2009. p. 381–408.
6. Abdelgaied A, Liu F, Brockett C, Jennings L, Fisher J, Jin Z. Computational wear prediction of artificial knee joints based on a new wear law and formulation. J Biomech. 2011;44:1108–16.
7. Abdelgaied A, Fisher J, Jennings LM. A comprehensive combined experimental and computational framework for pre-clinical wear simulation of total knee replacements. J Mech Behav Biomed Mater. 2018;78:282–91.
8. Fregly BJ, Sawyer WG, Harman MK, Banks SA. Computational wear prediction of a total knee replacement from in vivo kinematics. J Biomech. 2005;38:305–14.
9. Mell SP, Fullam S, Wimmer MA, Lundberg HJ. Finite element evaluation of the newest ISO testing standard for polyethylene total knee replacement liners. Proc Inst Mech Eng. 2018;232:545–52.
10. Taylor M, Prendergast PJ. Four decades of finite element analysis of orthopaedic devices: where are we now and what are the opportunities? J Biomech. 2015;48:767–78.
11. Pal S, Haider H, Laz PJ, Knight LA, Rullkoetter PJ. Probabilistic computational modeling of total knee replacement wear. Wear. 2008;264:701–7.
12. Viceconti M, Affatato S, Baleani M, Bordini B, Cristofolini L, Taddei F. Pre-clinical validation of joint prostheses: a systematic approach. J Mech Behav Biomed Mater. 2009;2:120–7.
13. Taylor WR, Schütz P, Bergmann G, List R, Postolka B, Hitz M, et al. A comprehensive assessment of the musculoskeletal system: the CAMS-Knee data set. J Biomech. 2017;65:32–9.
14. Dreyer MJ, Trepczynski A, Hosseini Nasab SH, Kutzner I, Schütz P, Weisse B, et al. European Society of Biomechanics S.M. Perren Award 2022: standardized tibio-femoral implant loads and kinematics. J Biomech. 2022;141:111171.

15. ISO. ISO 14243-1:2009. Implants for surgery - Wear of total knee-joint prostheses - Part 1: Loading and displacement parameters for wear-testing machines with load control and corresponding environmental conditions for test. Geneva: ISO; 2009 Nov. Available from: https://www.iso.org/standard/44262.html.
16. ASME. ASME V&V 40-2018. Assessing Credibility of Computational Modeling through Verification and Validation: Application to Medical Devices. New York: American Society of Mechanical Engineers; 2018 Nov. Available from: https://www.asme.org/products/codes-standards/vv-40-2018-assessing-credibility-computational#.
17. FDA. Assessing the Credibility of Computational Modeling and Simulation in Medical Device Submissions-Draft Guidance for Industry and Food and Drug Administration Staff. 2021 Dec. Available from: https://www.fda.gov/regulatory-information/search-fda-guidance-documents/assessing-credibility-computational-modeling-and-simulation-medical-device-submissions.
18. Okazaki Y, Hosoba M, Miura S, Mochizuki T. Effects of knee simulator control method and radiation dose on UHMWPE wear rate, and relationship between wear rate and clinical revision rate in National Joint Registry. J Mech Behav Biomed Mater. 2019;90:182–90.
19. Trepczynski A, Kutzner I, Schütz P, Dymke J, List R, von Roth P, et al. Tibio-femoral contact force distribution is not the only factor governing pivot location after total knee arthroplasty. Sci Rep. 2019;9:182.
20. Wang X-H, Li H, Dong X, Zhao F, Cheng C-K. Comparison of ISO 14243–1 to ASTM F3141 in terms of wearing of knee prostheses. Clin Biomech. 2019;63:34–40.
21. Kang L, Galvin AL, Fisher J, Jin Z. Enhanced computational prediction of polyethylene wear in hip joints by incorporating cross-shear and contact pressure in additional to load and sliding distance: effect of head diameter. J Biomech. 2009;42:912–8.
22. Saikko V. Effect of contact pressure on wear and friction of ultra-high molecular weight polyethylene in multidirectional sliding. Proc Inst Mech Eng. 2006;220:723–31.
23. Abdelgaied A, Fisher J, Jennings LM. Understanding the differences in wear testing method standards for total knee replacement. J Mech Behav Biomed Mater. 2022;132: 105258.
24. Bauer L, Kistler M, Steinbrück A, Ingr K, Müller PE, Jansson V, et al. Different ISO standards' wear kinematic profiles change the TKA inlay load. Appl Sci. 2021;11:3161.
25. Knight LA, Pal S, Coleman JC, Bronson F, Haider H, Levine DL, et al. Comparison of long-term numerical and experimental total knee replacement wear during simulated gait loading. J Biomech. 2007;40:1550–8.
26. McEwen HMJ, Barnett PI, Bell CJ, Farrar R, Auger DD, Stone MH, et al. The influence of design, materials and kinematics on the in vitro wear of total knee replacements. J Biomech. 2005;38:357–65.
27. Lin Y-C, Haftka RT, Queipo NV, Fregly BJ. Surrogate articular contact models for computationally efficient multibody dynamic simulations. Med Eng Phys. 2010;32:584–94.
28. Shu L, Hashimoto S, Sugita N. Enhanced in-silico polyethylene wear simulation of total knee replacements during daily activities. Ann Biomed Eng. 2021;49:322–33.
29. Reinders J, Sonntag R, Vot L, Gibney C, Nowack M, Kretzer JP. Wear testing of moderate activities of daily living using in vivo measured knee joint loading. PLoS ONE. 2015;10: e0123155.
30. Abdel-Jaber S, Belvedere C, Mattia JSD, Leardini A, Affatato S. A new protocol for wear testing of total knee prostheses from real joint kinematic data: towards a scenario of realistic simulations of daily living activities. J Biomech. 2016;49:2925–31.
31. ASTM International. ASTM F3141-17a. Standard Guide for Total Knee Replacement Loading Profiles. West Conshohocken: ASTM International; 2017. Available from: http://www.astm.org/cgi-bin/resolver.cgi?F3141-17A.
32. Bergmann G, Bender A, Graichen F, Dymke J, Rohlmann A, Trepczynski A, et al. Standardized loads acting in knee implants. PLoS ONE. 2014;9: e86035.
33. Fregly BJ, Besier TF, Lloyd DG, Delp SL, Banks SA, Pandy MG, et al. Grand challenge competition to predict in vivo knee loads: grand challenge competition. J Orthop Res. 2012;30:503–13.
34. ASTM International. ASTM F732-17. Standard Test Method for Wear Testing of Polymeric Materials Used in Total Joint Prostheses. West Conshohocken: ASTM International; 2017. Available from: http://www.astm.org/cgi-bin/resolver.cgi?F732-17.
35. Brandt J-M, Charron KD, Zhao L, MacDonald SJ, Medley JB. Lubricant biochemistry affects polyethylene wear in knee simulator testing. Biotribology. 2021;27: 100185.
36. Zhang J, Chen Z, Gao Y, Zhang X, Guo L, Jin Z. Computational wear prediction for impact of kinematics boundary conditions on wear of total knee replacement using two cross-shear models. J Tribol. 2019;141: 111201.
37. ISO. ISO 14243–3:2014. Implants for surgery-Wear of total knee-joint prostheses - Part 3: Loading and displacement parameters for wear-testing machines with displacement control and corresponding environmental conditions for test. Geneva: ISO; 2014 Jan. Available from: https://www.iso.org/standard/56649.html.
38. Saikko V. Effect of contact area on the wear and friction of UHMWPE in circular translation pin-on-disk tests. J Tribol. 2017;139: 061606.
39. Godest AC, Beaugonin M, Haug E, Taylor M, Gregson PJ. Simulation of a knee joint replacement during a gait cycle using explicit finite element analysis. J Biomech. 2002;35:267–75.
40. O'Brien S, Luo Y, Wu C, Petrak M, Bohm E, Brandt J-M. Computational development of a polyethylene wear model for the articular and backside surfaces in modular total knee replacements. Tribol Int. 2013;59:284–91.
41. Carr BC, Goswami T. Knee implants—review of models and biomechanics. Mater Des. 2009;30:398–413.
42. Zhang J, Chen Z, Wang L, Li D, Jin Z. A patient-specific wear prediction framework for an artificial knee joint with coupled musculoskeletal multibody-dynamics and finite element analysis. Tribol Int. 2017;109:382–9.
43. Zhao D, Sakoda H, Sawyer WG, Banks SA, Fregly BJ. Predicting knee replacement damage in a simulator machine using a computational model with a consistent wear factor. J Biomech Eng. 2008;130: 011004.
44. Baykal D, Siskey RS, Haider H, Saikko V, Ahlroos T, Kurtz SM. Advances in tribological testing of artificial joint biomaterials using multidirectional pin-on-disk testers. J Mech Behav Biomed Mater. 2014;31:117–34.
45. Goreham-Voss CM, Hyde PJ, Hall RM, Fisher J, Brown TD. Cross-shear implementation in sliding-distance-coupled finite element analysis of wear in metal-on-polyethylene total joint arthroplasty: intervertebral total disc replacement as an illustrative application. J Biomech. 2010;43:1674–81.

46. Wang A. A unified theory of wear for ultra-high molecular weight polyethylene in multi-directional sliding. Wear. 2001;248:38–47.
47. Dreyer MJ, Taylor WR, Wasmer K, Imwinkelried T, Heuberger R, Weisse B, et al. Anomalous wear behavior of UHMWPE during sliding against CoCrMo under varying cross-shear and contact pressure. Tribol Lett. 2022;70:119.
48. Quinci F, Dressler M, Strickland AM, Limbert G. Towards an accurate understanding of UHMWPE visco-dynamic behaviour for numerical modelling of implants. J Mech Behav Biomed Mater. 2014;32:62–75.
49. Lee K-Y, Pienkowski D, Lee S. Dynamic compressive creep of extruded ultra-high molecular weight polyethylene. KSME Int J. 2003;17:1332–8.
50. Lee K-Y, Pienkowski D. Viscoelastic recovery of creep-deformed ultra-high molecular weight polyethylene (UHMWPE). In: Gsell R, Stein H, Ploskonka J, editors. Characterization and properties of ultra-high molecular weight polyethylene. Conshohocken: ASTM; 1998. p. 30–6.
51. Willing R, Kim IY. A holistic numerical model to predict strain hardening and damage of UHMWPE under multiple total knee replacement kinematics and experimental validation. J Biomech. 2009;42:2520–7.

Publisher's Note